Preparations and Photophysical Properties of Fused and Nonfused Thienyl Bridged MM (M = Mo or W) Quadruply Bonded Complexes

Malcolm H. Chisholm,*,[†] Pi-Tai Chou,*,[‡] Yi-Hsuan Chou,[†] Yagnaseni Ghosh,[†] Terry L. Gustafson,*,[†] and Mei-Lin Ho[‡]

Department of Chemistry, The Ohio State University, 100 West 18 Avenue, Columbus, Ohio 43210-1185, and Department of Chemistry, National Taiwan University, No. 1, Section 4, Roosevelt Road, Taipei 10617, Taiwan

A series of metal–metal quadruply bonded compounds $[(^tBuCO_2)_3M_2]_2(\mu\text{-TT})$ where TT = thienothiophenedicarboxylate and M = Mo, **1A**, and M = W, **1B** and $[(^tBuCO_2)_3M_2]_2(\mu\text{-DTT})$ where DTT = dithienothiophenedicarboxylate and M = Mo, **2A**, and M = W, **2B**, has been prepared and characterized by elemental analysis, ESI- and MALDI-TOF mass spectrometry and ^1H NMR spectroscopy. Their photophysical properties have also been investigated by steady-state absorption as well as transient absorption and emission spectroscopy. The optimized structures and the predicted low energy electronic transitions were obtained by DFT and time-dependent DFT calculations, respectively, on model compounds. These results, in combination with the respective properties of the compounds $[(^tBuCO_2)_3M_2]_2(\mu\text{-BTh})$ (BTh = 2,5′-bithienyldicarboxylate, M = Mo, **3A**, and M = W, **3B**), allow us to make a comprehensive comparison of the fused (compounds **1A**, **1B**, **2A**, and **2B**) and the nonfused thienyl (compounds **3A** and **3B**) dicarboxylate bridged compounds of molybdenum and tungsten. The electrochemical studies show singly oxidized radical cations that are valence trapped on the EPR time-scale and are classified as Class 1 (M = Mo) or Class 2 (M = W) on the Robin and Day scale for mixed valence compounds. The new compounds exhibit intense metal to bridge ligand charge transfer absorption bands in the far visible and near IR (NIR) region. Both molybdenum and tungsten complexes show dual emission, but for molybdenum, the phosphorescence is dominant while for tungsten the emission is primarily fluorescence. Femtosecond transient absorption spectroscopy shows that the relaxation dynamics of the S_1 states which have lifetimes of ~10 ps is dominated by intersystem crossing (ISC), leading to T_1 states that in turn possess long lifetimes, ~70 μs (M = Mo) or 3 μs (M = W). These properties are contrasted with the photophysical properties of conjugated organic systems incorporating metal ions of the later transition elements.

Introduction

Conjugated organic oligomers and polymers have attracted a great deal of interest over the past two decades due to their optoelectronic properties.[1–3] They represent a class of organic semiconductors that may be doped to become conducting and metallic-like.[4–7] They also find applications in electronic devices such as organic field effect transistors (OFETs),[8,9] organic light emitting diodes (OLEDs),[10] polymer light

* To whom correspondences should be addressed. E-mail: chisholm@chemistry.ohio-state.edu (M.H.C.); gustafson@chemistry.ohio-state.edu (T.L.G.); chop@ntu.edu.tw (P.-T.C.).

† The Ohio State University.
‡ National Taiwan University.

(1) Burroughes, J. H.; Bradley, D. D. C.; Brown, A. R.; Marks, R. N.; Mackay, K.; Friend, R. H.; Burns, P. L.; Holmes, A. B. *Nature (London, United Kingdom)* **1990**, *347*, 539.
(2) Kraft, A.; Grimsdale, A. C.; Holmes, A. B. *Angew. Chem., Int. Ed.* **1998**, *37*, 403.
(3) Skotheim, T. A., Elsenbaumer, R. L., Reynolds, J. R., Eds. *Handbook of Conducting Polymers, Second Edition, Revised and Expanded*; M. Dekker: New York, 1997; p 1112.
(4) Ajayaghosh, A. *Chem. Soc. Rev.* **2003**, *32*, 181.
(5) Chen, P.; Yang, G.; Liu, T.; Li, T.; Wang, M.; Huang, W. *Polym. Int.* **2006**, *55*, 473.
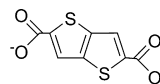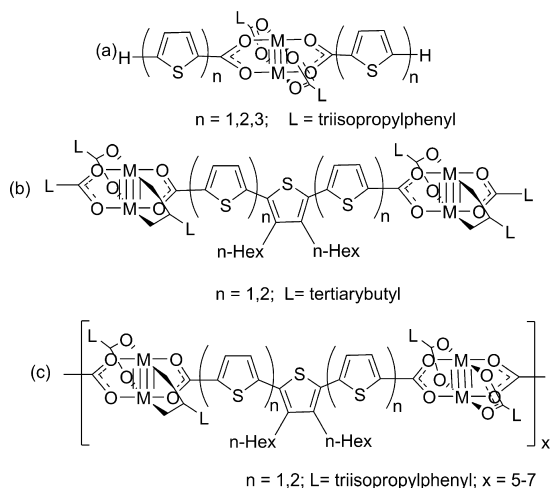(6) Wong, W.-Y.; Ho, C.-L. *Coord. Chem. Rev.* **2006**, *250*, 2627.
(7) Zade, S. S.; Bendikov, M. *J. Org. Chem.* **2006**, *71*, 2972.
(8) Locklin, J.; Roberts, M.; Mannsfeld, S.; Bao, Z. *Polym. Rev* **2006**, *46*, 79.
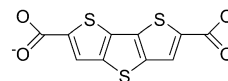(9) Yoon, M.-H.; Kim, C.; Facchetti, A.; Marks, T. J. *J. Am. Chem. Soc.* **2006**, *128*, 12851.
(10) Veinot Jonathan, G. C.; Marks Tobin, J. *Acc. Chem. Res.* **2005**, *38*, 632.
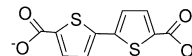
Scheme 1. Structures of (a) "bis−bis", (b) "dimers-of-dimers", and (c) oligomer compounds

(a) n = 1,2,3; L = triisopropylphenyl

(b) n = 1,2; L = tertiarybutyl

(c) n = 1,2; L= triisopropylphenyl; x = 5-7

Figure 1. Structures of thienothiophenedicarboxylate (TT), dithienothiophene-dicarboxylate (DTT), and bithienyldicarboxylate (BTh).

emitting devices (PLEDs),[11] photodiodes,[12] photoswitches,[12,13] etc., and several companies, including Cambridge Displays Technologies, Philips, and Seiko Epson, are pioneering their commercialization. Potential for commercialization arises from their synthetic flexibility, ease of processing by means of cheap technologies (spin-coating, ink-jet printing, and stamping) and the ability to change the physical properties of the polymer via the control of the molecular architecture.[1] Among the several classes of conjugated organic polymers, the poly(2,5-thiophenes) and their derivatives are particularly well studied due to their low band gaps and good hole transport properties. Their properties are, however, greatly modified by the dihedral angles between the adjacent rings and the introduction of alkyl groups at the 3 and 4 positions, which leads to increased solubility of the polymers/oligomers and reduces the degree of aromatic conjugation, hence increasing the band gap.[14–17] We have long been interested in the effect of incorporating MM quadruply bonded units (M = Mo or W) into oligothiophenes by the use of carboxylate linkers to effect $M_2\delta$ to thiophene conjugation.[18,19] Three classes of compounds have been studied and their corresponding structures are depicted in Scheme 1.

Compounds of the type *trans*-$M_2(TiPB)_2(O_2C-(Th)_n)_2$ (where n = 1, 2, and 3, TiPB = 2,4,6-tri-isopropylbenzoate, Th = thienyl) depicted as bis-bis and $[(Bu^tCO_2)_3M_2]_2(\mu-O_2C-(Th)_n(3,4-n-hexylTh)(Th)_nCO_2)$ depicted as dimers-of-dimers,

in Scheme 1, can be viewed as a prototype for the polymers/oligomers $[M_2(TiPB)_2(\mu-O_2C(Th)_n(3,4-n-hexylTh)(Th)_n-CO_2)]_x$ where n = 1 or 2. The introduction of the 3,4-*n*-hexyl thienyl units greatly increases the solubility of the metallated polymers/oligomers thus allowing spin-coating of thin films for device applications. However, as noted before, they also cause a twisting and hence decrease the conjugation along a chain.[20] In order to investigate and compare the properties of fused thienyl bridged complexes with those of nonfused thienyl bridged complexes,[18] we decided to prepare some model compounds having fused thiophene rings. Herein, we describe the preparation and salient photophysical properties of MM quadruply bonded complexes linked by thienothiophenedicarboxylate, TT, dithienothiophenecarboxylate, DTT, and bithienyldicarboxylate ligands, BTh, shown in Figure 1. The DTT and BTh bridges place the dinuclear centers at an equivalent distance apart, ∼15.00 (**2A**) and ∼14.56 Å (**3A**), estimated from density functional theory calculations (vide infra) but differ with respect to the planarity of the bridge.

Experimental Section

Measurements. NMR spectra were recorded on a 400 MHz Bruker DPX Advance400 spectrometer. All ^{1}H NMR chemical shifts are in ppm relative to the protio impurity in THF-d_8 at 3.58 ppm or DMSO-d_6 at 2.09 ppm.

Electronic spectra at room temperature were recorded using a Perkin-Elmer Lambda 900 spectrometer in THF solution. A 1.00 or 10.00 mm IR quartz cell was employed.

The cyclic voltammogram and differential pulse voltammogram of all the complexes were collected at a scan rate of 100 and 5 mV s^{-1} respectively, using a Princeton Applied Research (PAR) 173A potentiostat−galvanostat equipped with a PAR 176 current-to-voltage converter. Electrochemical measurements were performed under an inert atmosphere in a 0.5 M solution of $^nBu_4NPF_6$ in THF inside a single compartment voltammetric cell equipped with a platinum working electrode, a platinum wire auxiliary electrode, and a pseudoreference electrode consisting of a silver wire in 0.5 M $^nBu_4NPF_6$/THF separated from the bulk solution by a Vycor™ tip. The potential values are referenced to the FeCp$_2$/FeCp$_2^+$ couple, obtained by addition of a small amount of FeCp$_2$ to the solution.

(11) Perepichka, I. F.; Perepichka, D. F.; Meng, H.; Wudl, F. *Adv. Mater.* **2005**, *17*, 2281.
(12) Bushby, R. J.; Lozman, O. R. *Curr. Opin. Colloid Interface Sci.* **2002**, *7*, 343.
(13) Pierard, F.; Kirsch-De Mesmaeker, A. *Inorg. Chem. Commun.* **2006**, *9*, 111.
(14) Camaioni, N.; Ridolfi, G.; Fattori, V.; Favaretto, L.; Barbarella, G. *J. Mater. Chem.* **2005**, *15*, 2220.
(15) Matsumoto, K.; Fujitsuka, M.; Sato, T.; Onodera, S.; Ito, O. *J. Phys. Chem. B* **2000**, *104*, 11632.
(16) Milliron, D. J.; Alivisatos, A. P.; Pitois, C.; Edder, C.; Frechet, J. M. J. *Adv. Mater.* **2003**, *15*, 58.
(17) Otsubo, T.; Aso, Y.; Takimiya, K. *J. Mater. Chem.* **2002**, *12*, 2565.
(18) Byrnes, M. J.; Chisholm, M. H.; Clark, R. J. H.; Gallucci, J. C.; Hadad, C. M.; Patmore, N. J. *Inorg. Chem.* **2004**, *43*, 6334.
(19) Chisholm, M. H.; Epstein, A. J.; Gallucci, J. C.; Feil, F.; Pirkle, W. *Angew. Chem., Int. Ed.* **2005**, *44*, 6537–6540.

(20) Samuelson, E. J.; Mardalen, J. *The Handbook of Organic Conductive Molecules and Polymers*; Wiley: New York, 1996.

EPR measurements were made at the X-band (34 GHz) frequencies using a Bruker Elexys-500 spectrometer, equipped with an ER 051 QG bridge.

Steady-state and nanosecond photophysical measurements were carried out in 10.0×10.0 mm^2 square quartz cuvettes equipped with Kontes stopcocks, while a 5.0 mm quartz tube was used in the 77 K steady-state NIR emission, and a 10.0×2.0 mm cell was used in the femtosecond approach. The absorption spectra were measured with a Hewlett-Packard diode array spectrometer (HP 8453), and the corrected steady-state luminescence spectra were recorded on a SPEX Fluoromax-2 spectrofluorimeter in UV–vis region. The steady-state NIR-luminescence spectra were measured on a home-built instrument excited at 514 (Ar$^+$ laser) or 634 nm (He–Ne laser). The triplet emission lifetimes were also measured on the home-built instrument pumped by a frequency doubled (532 nm) or as an efficient optical parametric oscillator (OPO) crystal pumped by a Nd:YAG laser (700 nm, Continuum Surelite II Nd: YAG laser, fwhm ~8 ns, ~10 mJ per pulse), and the signal from the photomultiplier tube (Hamamatsu R928) was processed by a Tektronics 100 MHz oscilloscope (TDS 3012). Lifetime decays were fitted using OriginPro 7.0. To resolve the fluorescence at 700–900 nm for the Mo$_4$ complexes, an 8 ns pulse laser (450 nm, Ti-Sapphire laser, Lotis TII) coupled with a gateable intensified charge coupled detector (ICCD, Princeton Instrument, model 7467-0011) was applied, in which a detecting window of as small as ~10 ns was open right after the excitation pulse to eliminate the long-lived phosphorescence interference.

In the femtosecond transient absorption experiments, samples were excited at 420 (second harmonics) or 800 nm of a femtosecond Ti-sapphire oscillator (82 MHz, Spectra Physics) and monitored with a supercontinuum probe–pulse in the spectral range of 500–800 nm. The recorded spectra were time-corrected for the chirp of the supercontinuum. All transient signals were linearly dependent on the excitation power. The time resolution of the system is 300 fs, as determined by the two-photon absorption of methanol in the sample cell.

Microanalysis was performed by Atlantic Microlab Inc. (**1A**, **2A**, and **3A**) and H. Kolbe Microanalytisches Laboratorium (**1B**, **2B**, and **3B**).

Matrix assisted laser desorption/ionization time-of-flight (MALDI-TOF) was performed on a Bruker Reflex III (Bruker, Breman, Germany) mass spectrometer operated in a linear, positive ion mode with an N$_2$ laser. Dithranol was used as the matrix and prepared as a saturated solution in THF. Allotments of matrix and sample were thoroughly mixed together; 0.5 mL of this was spotted on the target plate and allowed to dry.

Synthesis. All reactions were carried out under one atmosphere of oxygen-free UHP-grade argon using standard Schlenk techniques or under a dry and oxygen-free nitrogen atmosphere using standard glovebox techniques. All solvents were dried and degassed by standard methods and distilled prior to use. Dimolybdenum tetrapivalate,[21] ditungsten tetrapivalate,[22] thieno[3,2-*b*]thiophene-dicarboxylic acid (TTH$_2$),[23] thieno[3,2-*b*]thieno[2′,2′-*d*]thiophene-dicarboxylic acid (DTTH$_2$),[24] and 2,2′-bithiophene-5,5′-dicarboxylic acid (BThH$_2$)[25] were prepared according to literature procedures.

(21) Brignole, A. B.; Cotton, F. A. *Inorg. Syn.* **1971**, *13*, 81.
(22) Santure, D. J.; Huffman, J. C.; Sattelberger, A. P. *Inorg. Chem.* **1985**, *24*, 371.
(23) Leriche, P.; Raimundo, J.-M.; Turbiez, M.; Monroche, V.; Allain, M.; Sauvage, F.-X.; Roncali, J.; Frere, P.; Skabara, P. J. *J. Mater. Chem.* **2003**, *13*, 1324.
(24) Frey, J.; Proemmel, S.; Armitage, M. A.; Holmes, A. B.; Takita, R.; Shibasaki, M. *Org. Synth.* **2006**, *83*, 209.
(25) Wang, S.; Brisse, F. *Macromolecules* **1998**, *31*, 2265.

n-Butyllithium (2.5 M in hexanes) was purchased from Acros and used as received. All manipulations of the studied compounds were performed in a nitrogen-filled glovebox or by using standard Schlenck line techniques in an atmosphere of oxygen-free UHP-grade argon and prepared with THF. THF dried over the appropriate drying agent was distilled prior to use and stored in reservoirs equipped with Kontes taps over activated 4 Å molecular sieves, under an argon atmosphere and degassed prior to use. The radical cations were generated in situ prior to EPR measurements, due to their instability, by treatment of all the neutral compounds with 0.75 equivalents of AgPF$_6$ in ether (**1A,B**; **2A,B**) and THF (**3A,B**).

[{(*t*BuCO$_2$)$_3$Mo$_2$}$_2${μ-TT}] (1A). Mo$_2$(O$_2$C*t*Bu)$_4$ (0.3490 g, 0.585 mmol) was dissolved in 30 mL of toluene, and this yellow solution was canulated to a Schlenk flask containing TTH$_2$ (0.0668 g, 0.293 mmol). The suspension was stirred at room temperature for 4 days, at the end of which, red precipitate dropped out. This was filtered via a frit, washed with toluene (2 × 10 mL) and finally with hexane (10 mL) before being dried in vacuo to give 250 mg (70% yield) of a red solid. Microanalysis found: C 37.51, H 4.64, S 5.27%. C$_{38}$H$_{56}$O$_{16}$S$_2$Mo$_4$ requires: C 37.25, H 4.77, and S 5.55%. NMR (THF-d_8): δ_H (400 MHz) 8.05 (s, 2H), 1.41 (s, 18H), 1.38 (s, 36H) ppm. MALDI-TOF: calculated monoisotopic MW for C$_{38}$H$_{56}$O$_{16}$S$_2$Mo$_4$: 1216.73. found: 1217.9 (M$^+$).

[{(*t*BuCO$_2$)$_3$W$_2$}$_2${μ-TT}] (1B). W$_2$(O$_2$C*t*Bu)$_4$ (0.3400 g, 0.432 mmol) was dissolved in 30 mL of toluene, and this yellow solution was canulated to a Schlenk flask containing TTH$_2$ (0.0350 g, 0.155 mmol). The suspension was stirred at room temperature for 6 days, at the end of which an indigo blue precipitate formed. This was filtered via a frit and washed with toluene (2 × 10 mL) and finally with hexane (10 mL) before being dried in vacuo to give 200 mg (59% yield) of a blue solid. Microanalysis found: C 29.04, H 3.57%. C$_{38}$H$_{56}$O$_{16}$S$_2$W$_4$ requires: C 29.10, H 3.60%. NMR (THF-d_8): δ_H (400 MHz) 7.41 (s, 2H), 1.40 (s, 18H), 1.36 (s, 36H) ppm. MALDI-TOF: calculated monoisotopic MW for C$_{38}$H$_{56}$O$_{16}$S$_2$W$_4$ 1568.33; found 1567.9 (M$^+$).

[{(*t*BuCO$_2$)$_3$Mo$_2$}$_2${μ-DTT}] (2A). The reaction was performed under similar conditions to those described for the preparation of **1A**, by using 0.5534 g of Mo$_2$(O$_2$C*t*Bu)$_4$ (0.928 mmol) and 0.1200 g of DTTH$_2$ (0.422 mmol). An orange red solid (425 mg, 72% yield) was isolated after 4 days of stirring at room temperature. Microanalysis found: C 37.59, H 3.83%. C$_{40}$H$_{56}$O$_{16}$S$_3$Mo$_4$ requires: C 37.75, H 4.43%. NMR (THF-d_8): δ_H (400 MHz) 8.04 (s, 2H), 1.43 (s, 18H), 1.41 (s, 36H) ppm. MALDI-TOF: calculated monoisotopic MW for C$_{40}$H$_{56}$O$_{16}$S$_3$Mo$_4$ 1272.82, found 1273.9 (M$^+$).

[{(*t*BuCO$_2$)$_3$W$_2$}$_2${μ-DTT}] (2B). The reaction was performed under similar conditions to those described for the preparation of **1B**, by using 0.5000 g of W$_2$(O$_2$C*t*Bu)$_4$ (0.647 mmol) and 0.0837 g of DTT (0.294 mmol). A greenish blue solid (320 mg, 61% yield) was isolated after 7 days of stirring at room temperature. Microanalysis found: C 29.65, H 3.36%. C$_{40}$H$_{56}$O$_{16}$S$_3$W$_4$ requires: C 29.58, H 3.47%. NMR (THF-d_8): δ_H (400 MHz) 8.07 (s, 2H), 1.42 (s, 18H), 1.40 (s, 36H) ppm. MALDI-TOF: calculated monoisotopic MW for C$_{40}$H$_{56}$O$_{16}$S$_3$W$_4$ 1624.42, found 1623 (M$^+$).

[{(*t*BuCO$_2$)$_3$Mo$_2$}$_2${μ-BTh}] (3A). The reaction was performed under similar conditions to those described for the preparation of **1A**, by using 0.5000 g of Mo$_2$(O$_2$C*t*Bu)$_4$ (0.838 mmol) and 0.1070 g of BThH$_2$ (0.421 mmol). A red solid (340 mg, 66% yield) was isolated after 4 days of stirring at room temperature. Microanalysis found: C 38.27, H 4.45%. C$_{40}$H$_{56}$O$_{16}$S$_2$Mo$_4$ requires: C 38.66, H 4.70%. NMR (THF-d_8): δ_H (400 MHz) 7.69 (d, 2H, J_{HH} = 4 Hz), 7.38 (d, 2H, J_{HH} = 4 Hz), 1.42 (s, 18H), 1.40 (s, 36H) ppm.

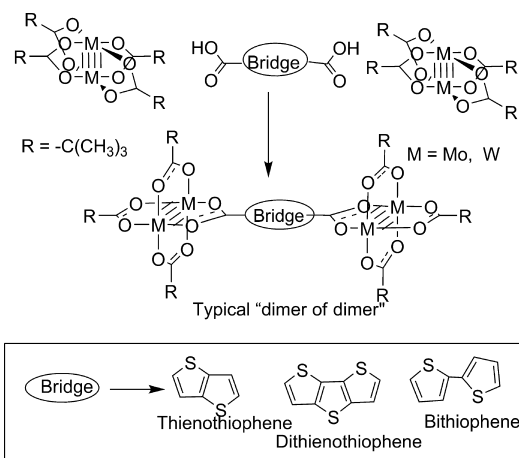MALDI-TOF: calculated monoisotopic MW for $C_{40}H_{58}O_{16}S_2Mo_4$ 1242.77, found 1243.5 (M^+).

[{($^tBuCO_2$)$_3W_2$}$_2${μ-BTh}] (3B). The reaction was performed under similar conditions to those described for the preparation of **1B**, by using 0.4120 g of $W_2(O_2C^tBu)_4$ (0.534 mmol) and 0.0690 g of BTh (0.267 mmol). A blue solid (220 mg, 52% yield) was isolated after 7 days of stirring at room temperature. Microanalysis found: C 30.58, H 3.78%. $C_{40}H_{58}O_{16}S_2W_4$ requires: C 30.13, H 3.67%. NMR (THF-d_8): δ_H (400 MHz) 7.31 (d, 2H, $J_{HH} = 4$ Hz), 7.20 (d, 2H, $J_{HH} = 4$ Hz), 1.43 (s, 18H), 1.40 (s, 36H) ppm.

Theoretical Approaches. Electronic structure calculations on the model compounds of the type [(HCO_2)_3M_2]_2(μ-X) where X = TT, DTT, and BTh and M = Mo and W were performed using density functional theory (DFT)[26–29] with the aid of the Gaussian03 suite of programs.[30] The B3LYP[31,32] exchange correlation functional was used along with the 6-31G* basis set for C, H, and O, 6-31+G (2d) basis set for S, and the SDD energy consistent pseudopotentials for molybdenum and tungsten. Geometry optimizations were performed in appropriate symmetry and were confirmed as local minima on the potential energy surfaces using frequency analysis. Pivalate groups were substituted by formate groups to reduce calculation time. Orbital analyses were preformed using Gaussview.[33] Time-dependent density functional theory was employed to predict optical transition spectra for the model complexes using same basis sets.[34–36] Calculations were also performed for the lowest energy triplet excited-state T_1, using the unrestricted B3LYP (UB3LYP) exchange correlation functional and the same basis sets.

Results and Discussion

Syntheses. The series of new compounds were synthesized from the reactions between the $M_2(O_2CBu^t)_4$ precursors and

(26) Hohenberg, P.; Kohn, W. *Phys. Rev.* **1964**, *136*, B864.
(27) Kohn, W.; Sham, L. J. *Phys. Rev.* **1965**, *137*, 1697.
(28) Parr, R. G.; Yang, W. *Density-functional Theory of Atoms and Molecules*; Oxford University Press: New York, 1989; p 333.
(29) Salahub, D. R., Zerner, M. C., Eds. In *The Challenge of d and f Electrons: Theory and Computation*; Proceedings of the 3rd Chemical Congress of North America, Toronto, Canada, June 5–11, 1988; ACS Symposium Series 394; American Chemical Society, Washington, D.C., 1989; p 405.
(30) Frisch, M. J.; Trucks, G. W.; Schlegel, H. B.; Scuseria, G. E.; Robb, M. A.; Cheeseman, J. R.; Montgomery, J. A., Jr.; Vreven, T.; Kudin, K. N.; Burant, J. C.; Millam, J. M.; Iyengar, S. S.; Tomasi, J.; Barone, V.; Mennucci, B.; Cossi, M.; Scalmani, G.; Rega, N.; Petersson, G. A.; Nakatsuji, H.; Hada, M.; Ehara, M.; Toyota, K.; Fukuda, R.; Hasegawa, J.; Ishida, M.; Nakajima, T.; Honda, Y.; Kitao, O.; Nakai, H.; Klene, M.; Li, X.; Knox, J. E.; Hratchian, H. P.; Cross, J. B.; Bakken, V.; Adamo, C.; Jaramillo, J.; Gomperts, R.; Stratmann, R. E.; Yazyev, O.; Austin, A. J.; Cammi, R.; Pomelli, C.; Ochterski, J. W.; Ayala, P. Y.; Morokuma, K.; Voth, G. A.; Salvador, P.; Dannenberg, J. J.; Zakrzewski, V. G.; Dapprich, S.; Daniels, A. D.; Strain, M. C.; Farkas, O.; Malick, D. K.; Rabuck, A. D.; Raghavachari, K.; Foresman, J. B.; Ortiz, J. V.; Cui, Q.; Baboul, A. G.; Clifford, S.; Cioslowski, J.; Stefanov, B. B.; Liu, G.; Liashenko, A.; Piskorz, P.; Komaromi, I.; Martin, R. L.; Fox, D. J.; Keith, T.; Al-Laham, M. A.; Peng, C. Y.; Nanayakkara, A.; Challacombe, M.; Gill, P. M. W.; Johnson, B.; Chen, W.; Wong, M. W.; Gonzalez, C.; Pople, J. A. *Gaussian 03*, revision C.02; Gaussian, Inc.: Wallingford, CT, 2004.
(31) Becke, A. D. *Phys. Rev. A: At. Mol. Opt. Phys.* **1988**, *38*, 3098.
(32) Miehlich, B.; Savin, A.; Stoll, H.; Preuss, H. *Chem. Phys. Lett.* **1989**, *157*, 200.
(33) Dennington, R. K. T.; Millam, J.; Eppinnett, K.; Hovell, W. L.; Gilliland, R. *GaussView*, version 3.09; Semichem, Inc.: Shawnee Mission, KS, 2003.
(34) Bauernschmitt, R.; Ahlrichs, R. *Chem. Phys. Lett.* **1996**, *256*, 454.
(35) Casida, M. E.; Jamorski, C.; Casida, K. C.; Salahub, D. R. *J. Chem. Phys.* **1998**, *108*, 4439.
(36) Stratmann, R. E.; Scuseria, G. E.; Frisch, M. J. *J. Chem. Phys.* **1998**, *109*, 8218.

Scheme 2. Illustration of the synthetic aim in this study

the respective dicarboxylic acids as shown in Scheme 2. The pale yellow toluene solutions of $M_2(O_2CBu^t)_4$ rapidly darkened as the reactions proceeded and the new compounds were formed as fine powders, being only very sparingly soluble in toluene. The molybdenum complexes [(Bu^tCO_2)$_3$-Mo_2]$_2$(μ-TT), **1A**, and [(Bu^tCO_2)$_3Mo_2$]$_2$(μ-DTT), **2A**, were bright orange or red while their respective tungsten analogues **1B** and **2B** were blue. All the compounds were air-sensitive and soluble in THF and other donor solvents such as DMSO. They showed molecular ions by MALDI-TOF mass spectrometry and their ^1H NMR spectra were consistent with expectations.

Electrochemical Studies. The prepared compounds have been examined by cyclic voltammetry and differential pulse voltammetry. All of the molybdenum containing compounds show a single reversible or quasi-reversible oxidation close to the $Cp_2Fe^{0/+}$ couple in THF solutions with $^nBu_4NPF_6$ as counter electrolyte. The tungsten complexes, in contrast, are notably easier to oxidize and show two reversible or quasi-reversible oxidations as shown in Figure 2. In each instance, we assign these oxidations as being M_2 based corresponding to removal of an electron from an $M_2\delta$ orbital and this is supported by both the EPR spectra and the predictions of electronic structure based on DFT calculations (vide infra).

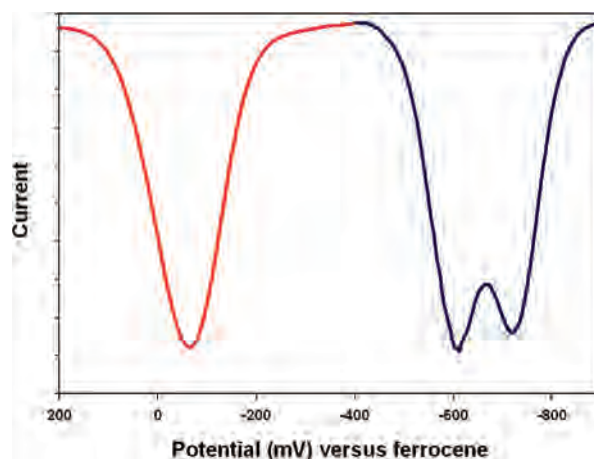**Figure 2.** Differential pulse voltammogram (DPV) for [($^tBuCO_2$)$_3Mo_2$]$_2$(μ-DTT) (red) and [($^tBuCO_2$)$_3W_2$]$_2$(μ-DTT) (blue) in a 0.1 M $^nBu_4NPF_6$/THF solution. Potentials are referenced to the $FeCp_2^{0/+}$ couple.

The presence of a single oxidation wave corresponding to the removal of two electrons for the molybdenum complexes is a clear indication of valence trapped behavior and the property of a Class I mixed valence compound on the Robin and Day classification scheme.[37] For the tungsten compounds the separation between the first and second oxidation potentials follows the order **1B** (182) > **2B** (108) > **3B** (90 mV), indicative of the influence of both W_2 to W_2 distance, **1B** (12.93) < **2B** (13.76) < **3B** (14.55 Å), and the greater coupling within the fused ring compounds. In the Robin and Day scheme, these compounds can reasonably be assigned as Class II. In contrast, the complex $[(Bu^tCO_2)_3W_2]_2(\mu\text{-}2,5\text{-}Th(CO_2)_2)$ containing a single thienyl ring, which brings the W_2 to W_2 distance to 10 Å, shows two oxidation waves separated by 310 mV, and the singly oxidized radical cation has been assigned as fully delocalized or Class III in the Robin and Day scheme based on UV–vis NIR and EPR data.[18]

EPR Studies. Supplementary support of the previous assignment is given by the EPR spectra. Oxidation of the neutral compounds with 0.75 equiv of $AgPF_6$ yields radical cations that are kinetically labile and decompose within hours at room temperature. Nevertheless, these radical cations are sufficiently persistent for studies by EPR spectroscopy in diethyl ether and THF at -50 °C. The molybdenum complex **1A**$^+$ showed an isotropic spectrum at -50 °C consisting of a central resonance at $g \sim 1.94$ flanked by a satellite spectrum of 6 lines due to the hyperfine coupling with $^{95/97}$Mo nuclei that have $I = ^5/_2$, a similar magnetic moment, and a combined natural abundance of $\sim 25\%$. The magnitude of the hyperfine coupling, A_0, was ~ 27 G which is typical for a $Mo_2(O_2CR)_4^+$ cation and together with the integral intensities of the hyperfine spectrum was indicative of a valence trapped radical. Under similar conditions, the tungsten complex ion **1B**$^+$ showed an isotropic spectrum consisting of a central signal, $g \sim 1.81$, flanked by satellites due to coupling to ^{183}W, $I = ^1/_2$, 14.5% natural abundance. The magnitude of the hyperfine coupling to ^{183}W, A_0, was 53 G, typical of a $W_2(O_2CR)_4^+$ ion which taken together with the relative intensities of the hyperfine spectrum once again indicated the valence trapped nature of the unpaired electron on the EPR time scale. In contrast, the spectrum of the radical cation of $[(Bu^tCO_2)_3W_2]_2(\mu\text{-}2,5\text{-}Th(CO_2)_2)$ formed upon oxidation with $AgPF_6$ showed evidence for complete delocalization of the unpaired electron over all four W atoms with $A_0 \sim 29$ G, $g = 1.83$.[18]

Electronic Absorption Spectra. The absorption spectra of molybdenum compounds **1A** and **2A** are shown in Figure 3, along with that of the bithienyldicarboxylate bridged compound $[(Bu^tCO_2)_3Mo_2]_2(\mu\text{-BTh})$, **3A**. All the compounds show an intense $S_0 \rightarrow S_1$ absorption band at around 530 nm that gives rise to their purple color in THF. This band originates from a metal-to-bridge ligand charge transfer (MLCT) mixed with some intraligand $\pi\text{-}\pi^*$ transition (LLCT) in character as anticipated by the nature of the HOMO and LUMO (Figure 10, vide infra). We anticipate
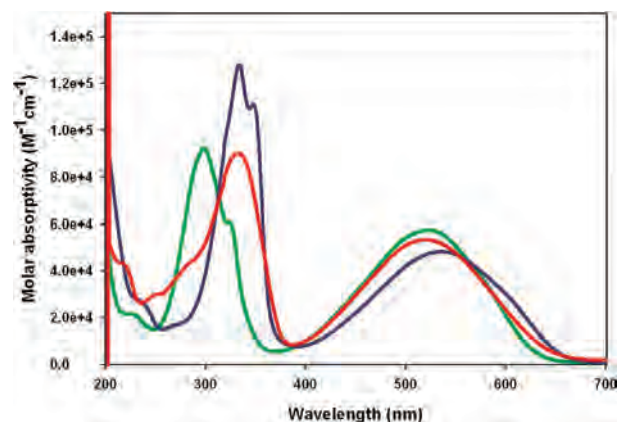
(37) Robin, M. B.; Day, P. *Adv. Inorg. Chem. Radiochem.* **1967**, *10*, 247.

Figure 3. Absorption spectra of molybdenum complexes $[(^tBuCO_2)_3Mo_2]_2(\mu\text{-}TT)$ (green), $[(^tBuCO_2)_3Mo_2]_2(\mu\text{-DTT})$ (blue), and $[(^tBuCO_2)_3Mo_2]_2(\mu\text{-BTh})$ (red) in THF.
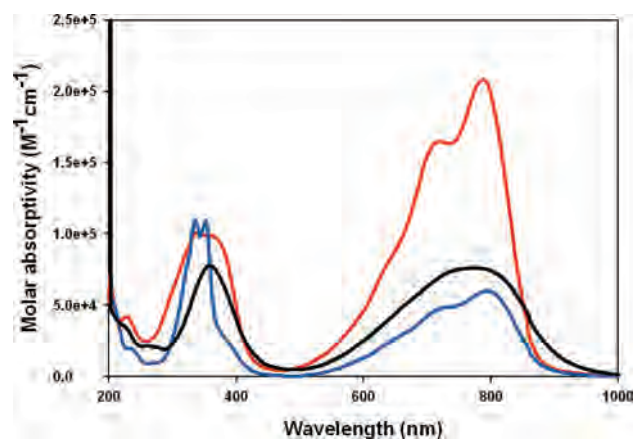

Figure 4. Absorption spectra of tungsten complexes $[(^tBuCO_2)_3W_2]_2(\mu\text{-}TT)$ (red), $[(^tBuCO_2)_3W_2]_2(\mu\text{-DTT})$ (blue), and $[(^tBuCO_2)_3W_2]_2(\mu\text{-BTh})$ (black) in THF.

that the change in color from orange-red in the solid state to purple in THF arises from solvation effects associated with these charge transfer absorptions.

Figure 4 shows the absorption spectra of the related tungsten compounds **1B**, **2B**, and **3B** in THF. The intense blue color of the THF solutions arises from the charge transfer bands that occur at around 700–800 nm. The intense absorption at ca. 300–350 nm present for both molybdenum and tungsten compounds (see Figures 2 and 3) originates predominantly from the fully allowed $\pi \rightarrow \pi^*$ transition of the bridge, together with $M_2\delta$ to $CO_2\pi^*$ transitions associated with the pivalate ligands. For the molybdenum complexes, there is a notable red shift on the $S_0 \rightarrow S_1$ peak wavelength between **1A** (520) and **2A** (540 nm). In contrast, a similar comparison between **1B** and **2B** reveals only a small (<5 nm) bathochromic shift. As supported by the higher molybdenum oxidation potential in cyclic voltammetry, the results may qualitatively be rationalized by a greater bridge $\pi\text{-}\pi^*$ contribution to the lowest lying singlet excited state in the molybdenum compounds. An increase of the fused ring from TT to DTT causes an elongation of the π-conjugation and a smaller $\pi\text{-}\pi^*$ energy gap; the π^* orbital is lowered in energy while the filled π is raised. Thus, for the $S_0 \rightarrow S_1$ transition with a greater MLCT/$\pi\text{-}\pi^*$ mixing character, a spectral red shift from **1A** to **2A** is reasonably expected. In contrast, for
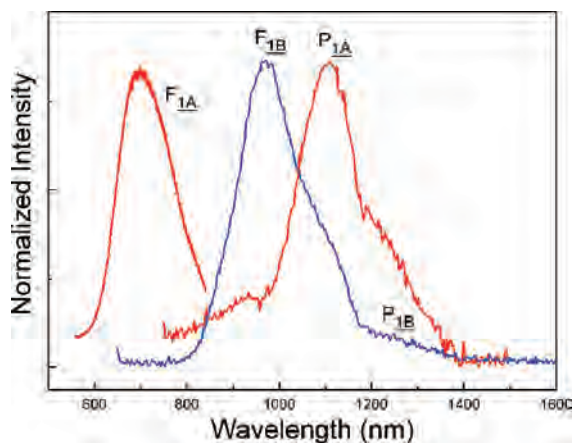
Figure 5. Emission spectra of **1A** = [(^{t}BuCO$_2$)$_3$Mo$_2$]$_2$(μ-TT) (red) (F_{1A}: fluorescence, P_{1A}: phosphorescence) and **1B** = [(^{t}BuCO$_2$)$_3$W$_2$]$_2$(μ-TT) (blue) (F_{1B}: fluorescence, P_{1B}: phosphorescence) in N$_2$ filled (1 atm) THF at room temperature. The excitation wavelength is the S$_0$−S$_1$ absorption peak wavelength (see Figures 2 and 3). Note that the fluorescence of [(^{t}BuCO$_2$)$_3$Mo$_2$]$_2$(μ-TT) was acquired from a time-gated (10 ns) intensified charge coupled detector (see text).

Figure 6. Phosphorescence spectra of [(^{t}BuCO$_2$)$_3$Mo$_2$]$_2$(μ-TT) (black), [(^{t}BuCO$_2$)$_3$Mo$_2$]$_2$(μ-DTT) (red), and [(^{t}BuCO$_2$)$_3$Mo$_2$]$_2$(μ-BTh) (green). (inset) Corresponding fluorescence spectra. All measurements were performed in N$_2$ (1 atm) filled THF at room temperature. The term λ_{ex} is the absorption peak wavelength.

the tungsten compounds where the S$_0$ → S$_1$ transition is dominated by M$_2$$\delta$ → bridge-π^*, the spectral shift may not be obvious due to the smaller contribution from the thiophene ligand π−π^* transition. We also note that for the same number of the thiophene rings, the nonfused compound **3A** (or **3B**) tends to have more diffusive spectral profile and red-shifted spectral onset region with respect to the fused compound **1A** (or **1B**) and **2A** (or **2B**), manifesting more rotational degrees of freedom for the nonfused **3A** (or **3B**) in the room temperature THF solution.

Luminescence. All the titled compounds exhibit far visible to near-infrared (NIR) emission in the region of 700–1400 nm, and a comparison of the emission spectra for the thienothiophenedicarboxylate bridged compounds **1A** versus **1B** is shown in Figure 5. In the steady-state measurement, **1A** emits primarily at 800 nm with a peak wavelength at ∼1100 nm. In comparison to the absorption maximum at ∼520 nm, it is very unlikely that the emission originates from the fluorescence. Time-resolved measurements further resolved a single decay component with a lifetime as long as ∼70 μs for the 1100 nm emission in the N$_2$ filled THF (1 atm, see the Experimental Section), confirming its assignment to a spin-forbidden transition, namely the phosphorescence. To resolve the presumably very weak and obscure fluorescence in **1A**, we further performed an experiment, in which the electronic gate of the intensified charge coupled detector (ICCD) was activated at within 10 ns after the excitation pulse to eliminate the phosphorescence interference. We then acquired the fluorescence with a peak wavelength at 710 nm for **1A** (see Figure 5). For the tungsten compound **1B**, the assignment of the 970 nm emission band to a fluorescence seems to be unambiguous owing to its rather short decay time (≪10 ns, vide infra) and well-correlated mirror image with respect to the S$_0$ → S$_1$ absorption band. Nevertheless, an obvious shoulder extending from 1200 to 1400 nm cannot be neglected. Upon monitoring at 1300 nm, in addition to a system response limited decay (<10 ns) that is attributed to the residue of the fluorescence, the NIR time-resolved
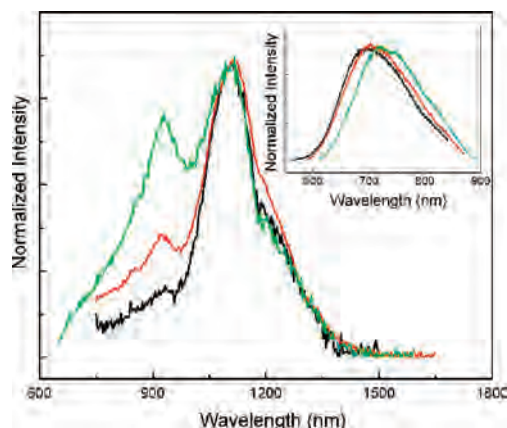
measurement (see the Experimental Section) resolved a much longer decay component with a lifetime of 3.5 μs. Accordingly, this ∼1300 nm emission band is reasonably assigned to a phosphorescence of **1B**.

Using the same methods as above, i.e. the steady-state NIR measurement coupled with the pulse-laser coupled ICCD time-resolved experiment, dual emission was clearly resolved for all the molybdenum compounds, consisting of a structureless fluorescence band maximized at 700–730 nm and a vibronically progressive phosphorescence band with the first peak wavelength at ∼950 nm. The fluorescence peak wavelength of **2A** (∼705) > **1A** (∼690 nm) is consistent with the trend observed in the S$_0$−S$_1$ absorption. However, despite the same absorption peak of ∼520 nm for **1A** and **3A**, the Stokes shift (peak-to-peak between absorption and emission) for the nonfused thienyl compound **3A** (λ_{em} ∼ 720 nm) is notably larger, as seen in Figure 6, manifesting its more significant change in geometry (toward the planar configuration) in the excited state. Monitored by the time-resolved NIR, the fluorescence decay was system response limited (<10 ns) for **1A**, **2A**, and **3A**, most probably indicating a fast rate of intersystem crossing assuming that other radiationless decay channels play minor roles. Detailed singlet excited-state relaxation dynamics will be elaborated in the section dealing with femtosecond transient absorption spectra, vide infra.

A comparison of the phosphorescence among molybdenum complexes **1A**, **2A**, and **3A** is depicted in Figure 6. Given the limitations of the NIR detector in the range 600–900 nm, we are not able to comment on the features seen in the spectra within this range except for the spectra shown in the insert which were obtained using an ICCD which itself is limited in the range 800–900 nm. The notion that we might be observing vibronic features can be dismissed on the basis that the apparent peak separation for compounds **3A** (green) and **2A** (red) is >1600 cm^{-1} which is not compatible with a symmetric stretching mode of the bridging thienyl dicarboxylate. The S$_1$−T$_1$ energy gap, which is taken by subtract-

(38) Turro, N. J. *Modern Molecular Photochemistry*; The Benjamin/Cummings: California, 1978.
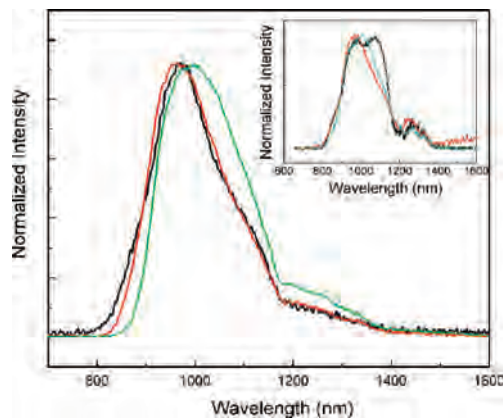
Figure 7. Emission spectra (fluorescence and phosphorescence) of $[(^tBuCO_2)_3W_2]_2(\mu\text{-}TT)$ (black), $[(^tBuCO_2)_3W_2]_2(\mu\text{-}DTT)$ (red), and $[(^tBuCO_2)_3W_2]_2(\mu\text{-}BTh)$ (green) measured in N_2 (1 atm) filled THF at room temperature. (insert) Corresponding emission spectra measured in the 77 K THF matrix. Note that the increase of >1500 nm emission in 77 K THF matrix for $[(^tBuCO_2)_3W_2]_2(\mu\text{-}BTh)$ is due to the stray light.

ing the phosphorescence (the lower energy peak) from the fluorescence in terms of energy, was calculated to be ∼10 kcal mol^{-1} which compares with a general energy gap of >15 kcal mol^{-1} for the pure $\pi\pi^*$ transition.[38]

Similar to the results of **1B** (see Figure 5), the room temperature fluorescence and phosphorescence were not well resolvable in **2B** and **3B**. Nevertheless, as shown in Figure 7, all tungsten compounds exhibit a distinct fluorescence band maximized at 970–1000 nm, accompanied by a shoulder around 1300 nm. The phosphorescence was further resolved to reveal a peak wavelength at ∼1250 nm in the 77 K THF matrix (see insert of Figure 7). Among the tungsten compounds, **3B** exhibits the longest fluorescence peak wavelength at ∼1000 nm, the result of which is consistent with a trend observed in the S_0-S_1 absorption (vide supra). Further estimation rendered an S_1-T_1 energy gap of <7.0 kcal mol^{-1} for all tungsten compounds, which is notably smaller than those observed for the molybdenum compounds.

Transient Absorption Spectroscopy. To gain further insight into the excited-state relaxation dynamics, femtosecond transient absorption measurements were performed for each compound. As a prototypical illustration, the resulting temporal evolution of the transient absorption for **2A** and **2B** and their corresponding rise and decay traces are depicted in Figures 8 and 9, respectively.

As shown in Figures 8 and 9, **2A** and **2B** reveal distinct transient absorption bands maximized at 650 and 520 nm, respectively. The corresponding relaxation dynamics for both **2A** and **2B** can be well-described by a system response-limited rise (∼350 fs), followed by a picosecond decay component, which was fitted to be 11.5 ± 0.4 (**2A**) and 12 ± 0.4 ps (**2B**) in THF. Finally, a nonzero constant component was resolved for both compounds in the detecting range of 50 ps. Note that the Franck–Condon excitation wavelength to prepare Figures 8 and 9 is 420 nm, which is well above the S_1 level, i.e. the S_n ($n > 1$) perhaps with a LLCT ($\pi-\pi^*$) character. Therefore, the $S_n \rightarrow S_1$ relaxation dynamics, namely the internal conversion, has to be considered. For **2B**, an additional experiment was performed in which **2B** was excited at the lowest lying transition of 770 nm and the
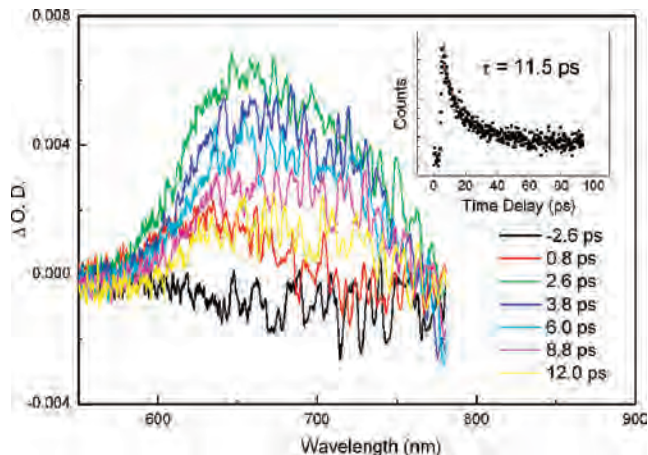

Figure 8. Transient absorption spectra of $[(^tBuCO_2)_3Mo_2]_2(\mu\text{-}DTT)$ as a function of various delay times. The measurements were performed in N_2 (1 atm) filled THF: λ_{ex} ∼420 nm. (inset) Corresponding rise and decay traces monitored at 650 nm.

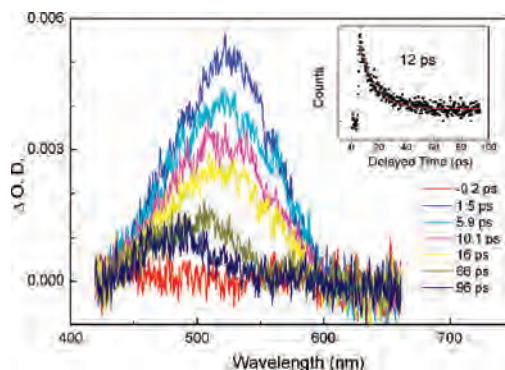**Figure 9.** Transient absorption spectra of $[(^tBuCO_2)_3W_2]_2(\mu\text{-}DTT)$ as a function of various delay times. The measurements were performed in N_2 (1 atm) filled THF: λ_{ex} ∼420 nm. (inset) Corresponding rise and decay traces monitored at 530 nm.

results (not shown here) showed negligible difference from that obtained at 420 nm, indicating an ultrafast $S_n \rightarrow S_1$ internal conversion (<350 fs) that is not necessary to be incorporated into the observed relaxation dynamics. Accordingly, the 11 ± 0.4 (**2A**) or 12 ± 0.4 ps (**2B**) component unambiguously corresponds to the decay of the S_1 state, i.e. the intersystem crossing leading to a population of the triplet manifold. The constant component that persists beyond 50 ps can thus be assigned to the decay of the T_1 state, and its associated $T_1 \rightarrow T_n$ absorption, being maximized at ∼700 and 500 nm for **2A** and **2B**, respectively, is slightly different from that of the respective $S_1 \rightarrow S_n$ transition. The lifetime of the T_1 state was further measured to be as long as microseconds by monitoring the phosphorescence decay dynamics. Table 1 lists the transient absorption peaks and the corresponding relaxation dynamics together with the population decay of the phosphorescence measured in THF.

As listed in Table 1, several salient features can be extracted and elaborated as follows. In comparison to most second and third row transition metal complexes with a mononuclear configuration, which normally undergo ultrafast $S_1 \rightarrow T_1$ ISC (<1 ps),[39] the relatively much slower (few to several tens of picoseconds) ISC for the titled complexes is

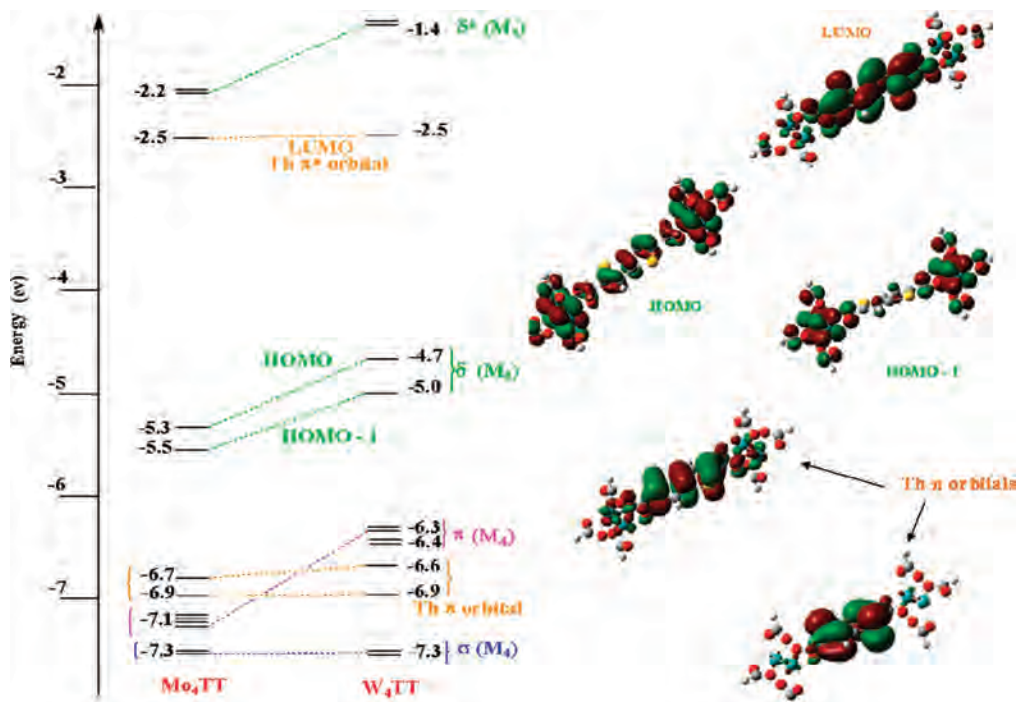(39) Chou, P. T.; Chi, Y. *Chem. Eur. J.* **2007**, *13*, 380.

Figure 10. Energy level diagram of frontier molecular orbitals for [(HCO$_2$)$_3$M$_2$]$_2$(μ-TT), model compound for [(^{t}BuCO$_2$)$_3$M$_2$]$_2$(μ-TT), when M = Mo and W. Selected frontier molecular orbital plots are calculated for [(HCO$_2$)$_3$Mo$_2$]$_2$(μ-TT). Note that the orbitals are drawn with an isosurface value of 0.02.

Table 1. Photophysical Data of Molybdenum and Tungsten Compounds in THF at Room Temperature[a]

compounds	λ_{abs}, nm ($\varepsilon \times 10^{-3}$) in M^{-1}cm^{-1}	λ_{em}, nm	$\lambda_{transient}$[b], nm	τ (S$_1$), ps $\pm$ 0.02	τ (T$_1$), μs
[(^{t}BuCO$_2$)$_3$Mo$_2$]$_2$(μ-TT)	525 (57.434)	690	655	7.9	69 $\pm$ 2.1
[(^{t}BuCO$_2$)$_3$Mo$_2$]$_2$(μ-DTT)	534 (48.400)	700	633	11	60 $\pm$ 2.1
[(^{t}BuCO$_2$)$_3$Mo$_2$]$_2$(μ-BTh)	520 (53.358)	720	620	8.6	72 $\pm$ 2.1
[(^{t}BuCO$_2$)$_3$W$_2$]$_2$(μ-TT)	790 (209.000)	960	c	c	4.0 $\pm$ 0.1
[(^{t}BuCO$_2$)$_3$W$_2$]$_2$(μ-DTT)	795 (61.714)	965	525	12	2.8 $\pm$ 0.1
[(^{t}BuCO$_2$)$_3$W$_2$]$_2$(μ-BTh)	790 (75.776)	980	526	14	3.6 $\pm$ 0.1

[a] All experiments were performed in the N$_2$ (1 atm) filled THF solution. [b] The peak wavelength of the transient absorption. [c] Not observed due to sample decomposition.

intriguing. It is possible the introduction of the carboxylate linker induces an adverse spin–orbit coupling between the M$_2$ and thienyl centers. Alternatively, the correlation between ISC rate and effective spin–orbit coupling distance may serve as another key factor. As a simplified approach based on the hydrogen-like atom, the rate of intersystem crossing is inversely proportional to r^6.[40] Although an analogous correlation can never be used for complicated molecules like the titled compounds, we can make a qualitative comparison. For example, monitored by the femtosecond transient absorption, the rate of intersystem crossing of **1A** (8) > **2A** (12 ps) can be rationalized by the increasing numbers of the fused thiophene moiety, hence lengthening the effective distance r between the metal center and the thiophene moiety. For both the multinuclear Mo and W complexes examined

in this study, the metal centered HOMO and thiophene based LUMO are bridged by a carboxylate functional group. This increase in separation is expected to reduce the rate of ISC and recently, the effect of distance tuning the ISC rate has been reported in several third-row transition metal complexes.[41–43]

It is also worthy of note that the long metal–ligand effective distance reduces the spin–orbit coupling and hence leads to the reduction of the S$_1$–T$_1$ state mixing. Accordingly, due to the reduced singlet-manifold contribution in T$_1$, the corresponding T$_1 \rightarrow$ S$_0$ transition is expected to be less favorable, resulting in a long radiative lifetime. This viewpoint is apparently applicable for the studied complexes. Taking the phosphorescence quantum yield, Φ_p, generally observed to be <0.01, the radiative lifetime τ_r, calculated via $\tau_r = \tau_{obs}/\Phi_p$, was deduced to be several to tens of milliseconds for all complexes studied. Such a long radiative lifetime is in sharp contrast to most Ir, Os, and Pt mononuclear complexes applied in OLEDs, for which a short radiative lifetime of e.g. < 10 μs is required to avoid any defect trapping prior to the charge recombination.[39]

Electronic Structure Calculations. To gain a more quantitative understanding of the bonding in these com-

(40) McGlynn, S. P.; Azumi, T.; Kinoshita, M. *Molecular Spectroscopy of the Triplet State*; International Series in Chemistry; Prentice-Hall: New York, 1969.

(41) Fernandez, I.; Sierra, M. A.; Gomez-Gallego, M.; Mancheno, M. J.; Cossio, F. P. *Chem. Eur. J.* **2005**, *11*, 5988.

(42) Lafolet, F.; Welter, S.; Popovic, Z.; De Cola, L. *J. Mater. Chem.* **2005**, *15*, 2820.

(43) Chen, Y.-L.; Lee, S.-W.; Chi, Y.; Hwang, K.-C.; Kumar, S. B.; Hu, Y.-H.; Cheng, Y.-M.; Chou, P.-T.; Peng, S.-M.; Lee, G.-H.; Yeh, S.-J.; Chen, C.-T. *Inorg. Chem.* **2005**, *44*, 4287.

Table 2. Comparison of Lowest Energy Transition (HOMO → LUMO) Calculated by TD-DFT for Model Compounds [(HCO$_2$)$_3$Mo$_2$]$_2$(μ-TT) and [(HCO$_2$)$_3$W$_2$]$_2$(μ-TT) with the Experimentally Observed MLCT Band for [(^{t}BuCO$_2$)$_3$Mo$_2$]$_2$(μ-TT) and [(^{t}BuCO$_2$)$_3$W$_2$]$_2$(μ-TT)

	λ_{calc} (nm)	ΔE_{calc} (eV)	f_{osc}	λ_{obs} (nm)	ΔE_{obs} (eV)	ε (M^{-1} cm^{-1})
[(^{t}BuCO$_2$)$_3$Mo$_2$]$_2$(μ-TT)	519	2.39	0.8	521	2.38	∼60 000
[(^{t}BuCO$_2$)$_3$W$_2$]$_2$(μ-TT)	619	2.66	1.0	715	1.73	∼200 000

pounds, we undertook electronic structure calculations employing density functional theory. In this approach the bulky pivalate ligands are replaced by formate groups to simplify the computational time. Such a truncation has been found to be useful in examining the electronic structures of bridged compounds of the form [(Bu^{t}CO$_2$)$_3$M$_2$]$_2$(μ-X) where M = Mo or W and X = oxalate,[44] perfluoroterephthalate and related aryldicarboxylates,[45] 2,5-thienyldicarboxylate,[18] and 2,6-azulenedicarboxylate.[46] The compounds **1(A,B)** were geometry optimized in C_{2h} symmetry while **2(A,B)** and **3(A,B)** were optimized in C_s and C_1 geometry, respectively. In the geometry optimized ground-state structures for **1(A,B)** and **2(A,B)**, it was found that the fused thiophene rings are planar with respect to the M$_2$ centers. This facilitates extended π delocalization and introduces greater M$_2\delta$−bridge π electronic coupling in these systems.

For the model compounds of **3A** and **3B**, however, the rings of the thiophene were found to be twisted by an angle of 148° resulting in a loss of planarity with the M$_2$ centers. This alludes to the fact that facile electron delocalization across the M$_2$ centers via the BTh bridge is hindered resulting in a lesser degree of electronic communication in these compounds.

The frontier molecular orbitals were plotted in Gaussview with isosurface value of 0.02, and it was found that, for all the compounds, the HOMO and HOMO − 1 were combinations of the M$_2$ δ and ligand π orbitals. The LUMO in each case was a thiophene based π* orbital. Time-dependent DFT calculations showed that the lowest energy transition primarily involved HOMO to LUMO transition as was verified experimentally from the absorption maxima and the high value of the extinction coefficient (Table 2).

The S$_0$ → S$_1$ energy gap for the calculated model compounds pertain to the model formate compounds in the gas phase while the experimental data pertain to pivalate complexes in THF. In spite of that, the close correlation between calculated and experimental values for the model compound of **1A** is highly encouraging. The much larger discrepancy between the predictions and the observed data for the tungsten complexes has been seen before in calculations[47] pertaining to bridged dicarboxylate compounds and presumably arises, at least in part, due to greater spin–orbit

(44) Bursten, B. E.; Chisholm, M. H.; D'Acchioli, J. S. *Inorg. Chem.* **2005**, *44*, 5571.

(45) Bursten, B. E.; Chisholm, M. H.; Clark, R. J. H.; Firth, S.; Hadad, C. M.; Wilson, P. J.; Woodward, P. M.; Zaleski, J. M. *J. Am. Chem. Soc.* **2002**, *124*, 12244.

(46) Barybin, M. V.; Chisholm, M. H.; Dalal, N. S.; Holovics, T. H.; Patmore, N. J.; Robinson, R. E.; Zipse, D. J. *J. Am. Chem. Soc.* **2005**, *127*, 15182.

(47) Chisholm, M. H.; Feil, F.; Hadad, C. M.; Patmore, N. J. *J. Am. Chem. Soc.* **2005**, *127*, 18150.
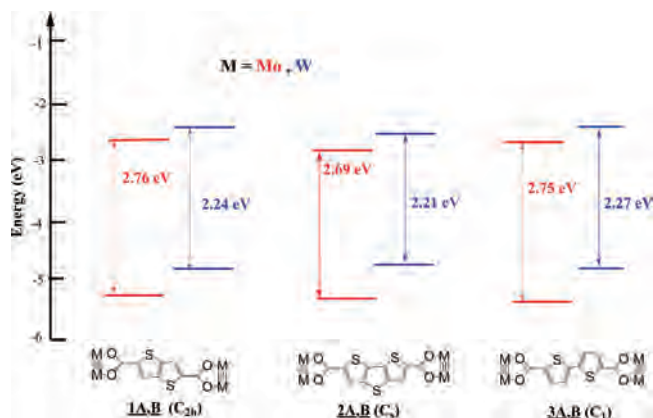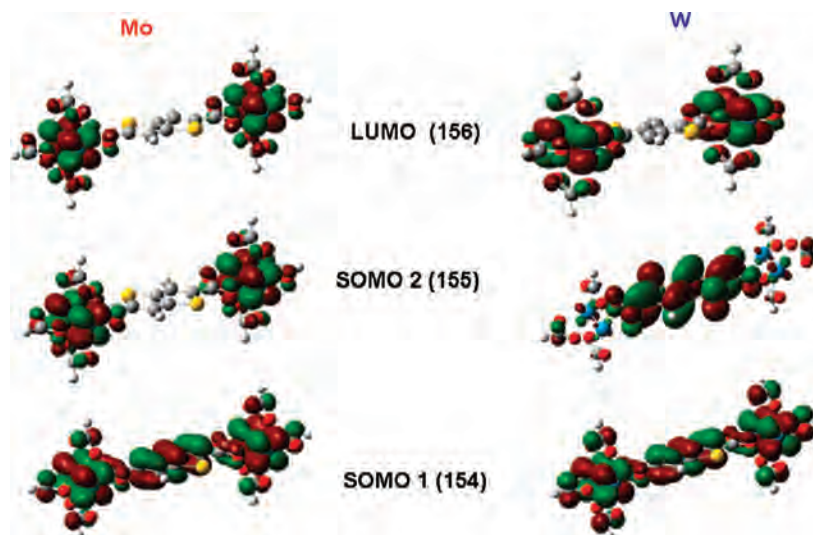
Figure 11. Calculated energy levels of the HOMO and LUMO for the model molybdenum and tungsten compounds.

coupling associated with the heavy third row transition element.

Figure 10 shows a comparison of the energy levels of the frontier molecular orbitals (FMOs) of the model compounds pertaining to **1A** and **1B** along with the Gaussview plots of selected FMO's of **1A**. Some of the salient features observed in this figure are described below.

The calculated HOMO and HOMO − 1 for the tungsten complex are relatively higher in energy than those of the molybdenum, while the LUMO which is primarily thiophene π* based remain essentially unchanged in energy. This observation is consistent with the results from cyclic voltammetry. Also the absorption spectra reveal the lower energy of the HOMO–LUMO transition for the tungsten complexes (vide supra) which points to the easier oxidation of the tungsten complexes. It is also worthy of mention that the calculations indicate that in all cases the LUMO is not an M$_2\delta$* combination and furthermore that the ordering of the bridge based filled π orbitals of highest energy (depicted in Figure 10) lie below the Mo$_2\delta$ combinations and above the Mo$_2\pi$'s. For tungsten, these filled thienyl π-orbitals fall between the W$_2\pi$ and W$_2\sigma$ combinations.

When comparing the various bridges, TT, DTT, and BTH, it was found that model compounds of **2(A,B)** showed the lowest energy gap between HOMO and LUMO while TT and BTh showed nearly similar gaps as seen in Figure 11. This is explained from the fact that DTT bridging ligand has three thiophene rings which are fused together and confined in the same plane as the M$_2$ centers. This results in the lowering of the thiophene π* orbitals and consequently reduces the energy gap. The lower number of fused rings in **1(A,B)** and the twisting of the thienyl rings in **3(A,B)** results in larger energy gap. This trend is observed in the lower oxidation potential of **2(A,B)** compared to **1(A,B)** which in turn is lower than **3(A,B)** [see the Supporting Information]. Furthermore, **2(A,B)** show the greatest red-shift in the absorption maxima of their lowest energy electronic transition, while a higher energy MLCT transition is seen for **1(A,B)** and the highest for **3(A,B)**.

Calculations were also performed on the lowest energy triplet state, T$_1$, of the model compounds. In all cases the geometries of the model formate complexes for **1A**, **1B**, **2A**, **2B**, **3A**, and **3B** were optimized and the frequency analysis

Figure 12. Gaussview plots of the frontier orbitals of the T_1 state of $[(HCO_2)_3M_2]_2(\mu\text{-TT})$, model compounds for $[(^tBuCO_2)_3M_2]_2(\mu\text{-TT})$, when M = Mo and W. The orbitals are drawn with an isosurface value of 0.02.

revealed that these were local minima on the potential energy surface. We have not done time dependent DFT calculations to attempt to correlate the energies of the emissive triplet states but rather have used these calculations to examine the formal nature of the states. For the molybdenum complexes **1A** and **3A**, the calculations suggest that the T_1 state is best described as a $^3MM(\delta\delta^*)$ state and the tungsten complex **3B** is similarly described. For the molybdenum complex **2A**, having three fused rings and for the tungsten complexes **1B** and **2B**, the T_1 state is ^3MLCT involving a metal δ combination and the bridge π^*. The difference between the molybdenum and tungsten complexes primarily owes its origin in the relative positioning of the $M_2\delta$ and δ^* manifolds. The relative energy of the bridge based π^* orbitals is primarily determined by the degree of conjugation which brings DTT (three fused rings) bridge to a lower energy than the others. For the bithiophene bridge, the dihedral angle between the two thiophene rings decreases the conjugation. A comparison of the calculated $^3MM(\delta\delta^*)$ and ^3MLCT states for the model compounds for **1A** and **1B** are represented by the Gaussview plots shown in Figure 12. Related Gaussview plots for the T_1 states of the model compounds for **2A**, **2B**, **3A**, and **3B** are shown in the Supporting Information.

Concluding Remarks

In conclusion, a new series of fused thienyl dicarboxylate bridged MM (M = Mo or W) quadruply bonded complexes has been prepared and associated electrochemical and photophysical properties investigated and compared with the previously reported nonfused thienyl complex.[18] On the basis of steady-state absorption/emission NIR time-resolved dynamics and femtosecond transient absorption studies, the associated photophysical properties can be generalized and depicted by using the simplified Jablonski diagram shown in Figure 13. Upon ^1LLCT excitation ultrafast (<350 fs) S_n (^1LLCT) → S_1 ($^1MLCT/\pi\pi^*$) internal conversion takes place, followed by a relatively slow (~ few to tens of picoseconds) S_1 ($^1MLCT/\pi\pi^*$) → T_1 intersystem crossing, giving rise to
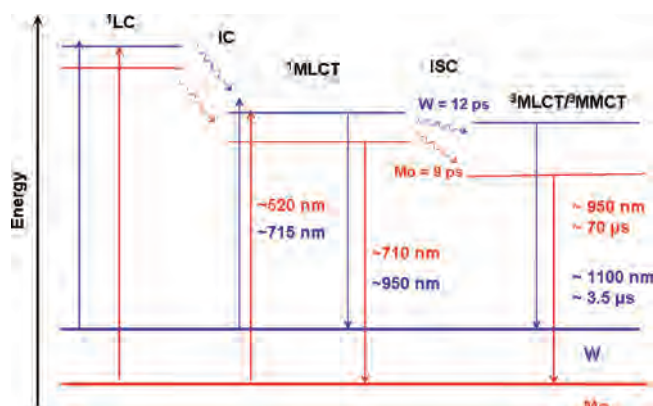

Figure 13. Jablonski diagram and the corresponding relaxation dynamics of the molybdenum and tungsten compounds applied in this study.

dual emission, i.e. fluorescence and phosphorescence. The lifetimes of phosphorescence were resolved to be within a few to tens of microseconds for all titled compounds. The calculations on the model compounds suggest that the nature of the T_1 states is dependent on both the metal and the bridge. This is clearly a very interesting suggestion and warrants further experimental work. We plan further studies involving time-resolved Raman and infrared spectroscopies to address these issues.

The majority of the work previously reported for metallated thiophene systems has involved the more electronegative late transition elements such as Au,[48] Pt,[49] Ru,[50] and Os.[51] In most of these systems, the lowest energy absorptions arise for ^1LLCT with some metal d orbital mixing because the highest occupied metal orbitals lie below those of the ligand. This is not the case for Ru (II) and Os (II) where the

(48) Li, P.; Ahrens, B.; Feeder, N.; Raithby, P. R.; Teat, S. J.; Khan, M. S. *Dalton Trans.* **2005**, *5*, 874.
(49) Khan, M. S.; Al-Mandhary, M. R. A.; Al-Suti, M. K.; Feeder, N.; Nahar, S.; Koehler, A.; Friend, R. H.; Wilson, P. J.; Raithby, P. R. *Dalton Trans.* **2002**, *12*, 2441.
(50) Liu, Y.; De Nicola, A.; Reiff, O.; Ziessel, R.; Schanze, K. S. *J. Phys. Chem. A* **2003**, *107*, 3476.
(51) Walters, K. A.; Trouillet, L.; Guillerez, S.; Schanze, K. S. *Inorg. Chem.* **2000**, *39*, 5496.

first oxidation is metal based and the lowest energy absorption is ^{1}MLCT.[50,51] However, this is very close in energy to LLCT and occurs at wavelength in the region 400–500 nm and the change in going from Ru to Os produces a very modest red shift. In our studies, we see much lower energy absorptions arising from ^{1}MLCT due to the higher energy of the M_2 δ orbitals. Furthermore, we observe a very significant red shift of 0.65 eV in going from the second row metal Mo to the third row metal W. Thus, the M_2 metallated thienyl carboxylates of molybdenum and tungsten having quadruple bonds may find applications in solar energy conversion due to their intense absorptions which span the region 300–800 nm (see Figures 3 and 4 and the Supporting Information) and their long-lived photoexcited states. Also, we note that in the systems reported here we observed both phosphorescence and fluorescence at room temperature. This is also quite unusual when compared to the metallated oligothiophenes of the later transition elements.[52] Given the growing interest in NIR emitters[53–55] with potential applications for night vision displays and sensors, we plan further studies on related systems.

Supporting Information Available: Listings of electrochemical data and computational calculations of triplet states of Mo and W complexes. This material is available free of charge via the Internet at http://pubs.acs.org.

IC800090N

(52) Wilson, J. S.; Chawdhury, N.; Al-Mandhary, M. R. A.; Younus, M.; Khan, M. S.; Raithby, P. R.; Koehler, A.; Friend, R. H. *J. Am. Chem. Soc.* **2001**, *23*, 9412.

(53) Harrison, B. S.; Foley, T. J.; Bouguettaya, M.; Boncella, J. M.; Reynolds, J. R.; Schanze, K. S.; Shim, J.; Holloway, P. H.; Padmanaban, G.; Ramakrishnan, S. *Appl. Phys. Lett.* **2001**, *79*, 3770.

(54) O'Riordan, A.; O'Connor, E.; Moynihan, S.; Nockemann, P.; Fias, P.; Van Deun, R.; Cupertino, D.; Mackie, P.; Redmond, G. *Thin Solid Films* **2006**, *497*, 299.

(55) Slooff, L. H.; Polman, A.; Cacialli, F.; Friend, R. H.; Hebbink, G. A.; van Veggel, F. C. J. M.; Reinhoudt, D. N. *Appl. Phys. Lett.* **2001**, *78*, 2122.